Electronic Supplementary Material (ESI) for Physical Chemistry Chemical Physics.


# Beyond Metals: Theoretical Discovery of Semiconducting MAX Phases and their Potential Application in Thermoelectrics

Mohammad Khazaei,[1] Iraj Maleki,[1] Namitha Anna Koshi,[2] Ahmad Ranjbar,[3] Nanxi Miao,[4] Junjie Wang,[4] Rasoul Khaledialidusti,[5] Thomas D. Kühne,[3] Seung-Cheol Lee,[6] Satadeep Bhattacharjee,[2] Hamid Hosano,[7,8] S. Mehdi Vaez Allaei,[1] Keivan Esfarjani,[9] and Kaoru Ohno[10]

[1]*Department of Physics, University of Tehran, North Kargar Ave., Tehran 14395-547, Iran*

[2]*Indo-Korea Science and Technology Center (IKST), Jakkur, Bengaluru 560065, India*

[3]*Dynamics of Condensed Matter and Center for Sustainable Systems Design, Theoretical Chemistry, University of Paderborn, Warburger Str. 100, D-33098 Paderborn, Germany*

[4]*State Key Laboratory of Solidification Processing, Northwestern Polytechnical University, Xi'an, Shaanxi 710072, People's Republic of China*

[5]*Department of Mechanical and Industrial Engineering, Norwegian University of Science and Technology (NTNU) Trondheim 7491, Norway*

[6]*Electronic Materials Research Center, KIST, Seoul 136-791, South Korea*

[7]*Graduate School of Science and Technology, Kumamoto University, Kumamoto 860-8555, Japan*

[8]*Department of Biomaterials and Bioelectrics, Institute of Industrial Nanomaterials, Kumamoto University, Japan*

[9]*Departments of Mechanical and Aerospace Engineering, Physics, and Materials Science and Engineering, University of Virginia, 122 Engineer's Way, Charlottesville, VA 22904, USA*

[10]*Department of Physics, Graduate School of Engineering Science, Yokohama National University, Yokohama 240-8501, Japan*

(Dated: June 17, 2024)

# Calculation of scattering rates and relaxation times

The momentum relaxation rate for acoustic deformation potential scattering is given by [1, 2]

$$\frac{1}{\tau_{ac}(k)} = \frac{e^2 k_B T E_D^2 k^2}{3\pi\hbar^2 c_{el} v(k)}[3 - 8c^2(k) + 6c^4(k)], \tag{S1}$$

where $c_{el}$ is the spherically averaged elastic constant and $E_D$ is acoustic deformation potential.

The momentum relaxation rate for ionized impurity scattering is given by [1, 2]

$$\frac{1}{\tau_{ii}(k)} = \frac{e^4 N}{8\pi\epsilon_0^2\hbar^2 k^2 v(k)}[D(k)ln(1 + \frac{4k^2}{\beta^2}) - B(k)], \tag{S2}$$

where $\epsilon_0$ is the dielectric constant, $\beta$ is the inverse screening length and N, the concentration of ionized impurity. The expressions for $\beta$, D(k) and B(k) are given in [3]. This scattering mechanism is important at low temperatures and high carrier concentrations. $\frac{1}{\tau_{el}(k)}$ is the sum of momentum relaxation rates of all elastic scattering processes considered (Matthiessen's rule) *i.e.* $\frac{1}{\tau_{el}(k)} = \frac{1}{\tau_{ac}(k)} + \frac{1}{\tau_{ii}(k)}$. For inelastic POP scattering, the *out scattering* operator $S_o$ is given by [1]

$$S_o = (N_{po} + 1 - f^-)\lambda_0^- + (N_{po} + f^+)\lambda_0^+ \tag{S3}$$

and the *in scattering* operator $S_i$ is given by [1]

$$S_i = (N_{po} + f)\lambda_i^- g^- + (N_{po} + 1 - f)\lambda_i^+ g^+ \tag{S4}$$

Here, $\lambda_o$ and $\lambda_i$ are the rates of *out* scattering and *in scattering* respectively. The expressions for which are provided in [3]. Also, the subscript plus and minus denotes the scattering by absorption or emission respectively. $N_{po}$ is the number of phonons and is given by [1]

$$N_{po} = \frac{1}{exp(\hbar\omega_{po}/k_B T) - 1}. \tag{S5}$$

The POP scattering rate is calculated iteratively using Rode's formalism.

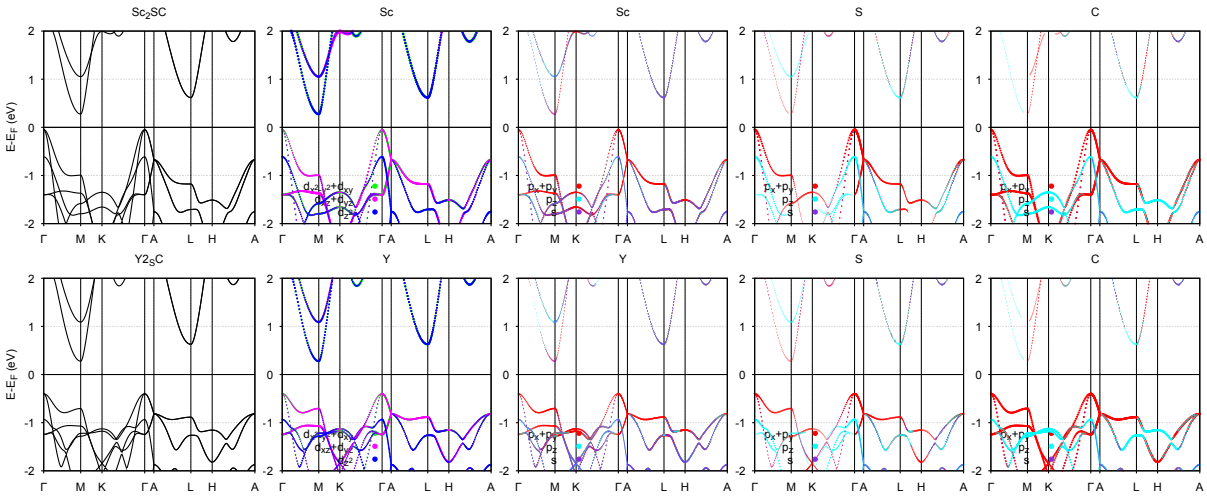


HSE06 orbitally projected band structures for $Sc_2SC$, and $Y_2SC$ MXenes

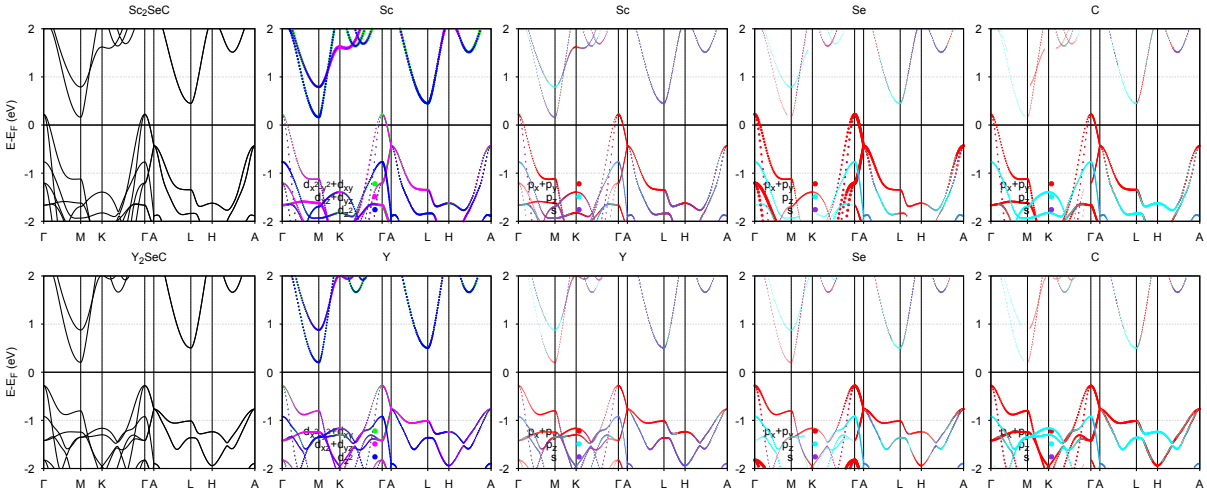


HSE06 orbitally projected band structures for $Sc_2SeC$, and $Y_2SeC$ MXenes

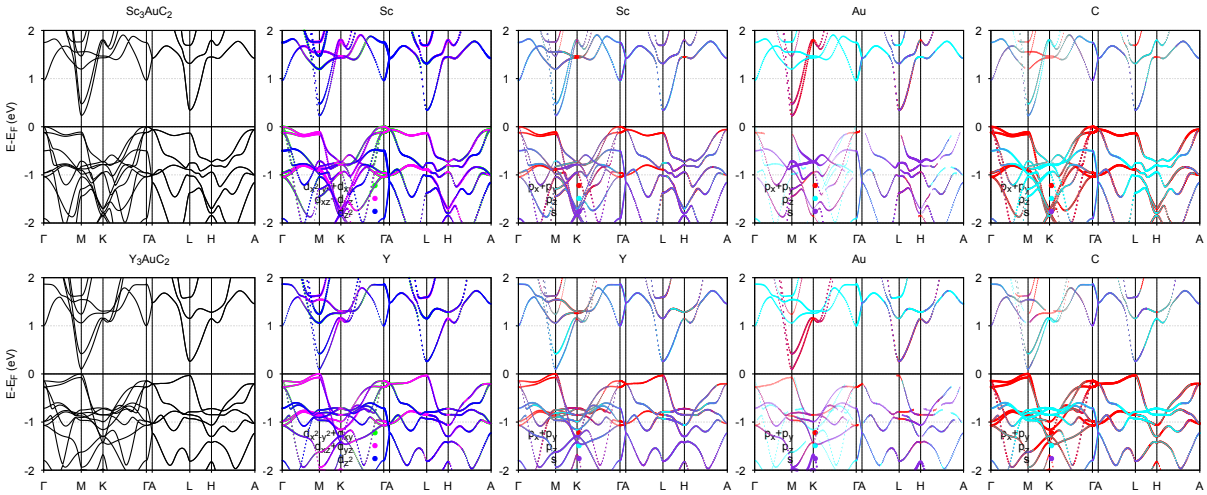


HSE06 orbitally projected band structures for $Sc_3AuC_2$, and $Y_3AuC_2$ MXenes

FIG. S1: The HSE06 functional projected band structures for all structures..

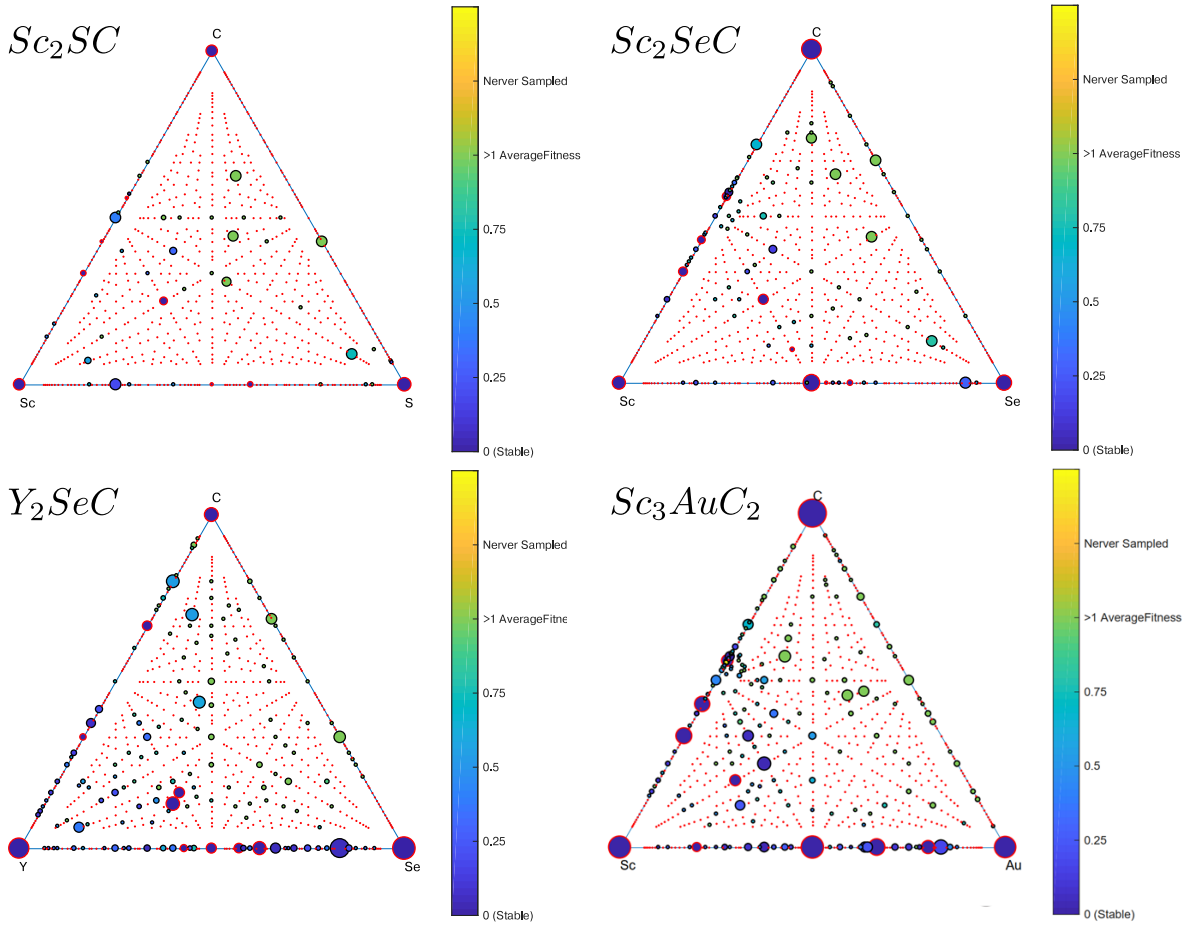


FIG. S2: Ternary phase diagrams for $Sc_2SC$, $Sc_2SeC$, $Y_2SeC$, and $Sc_3AuC_2$.

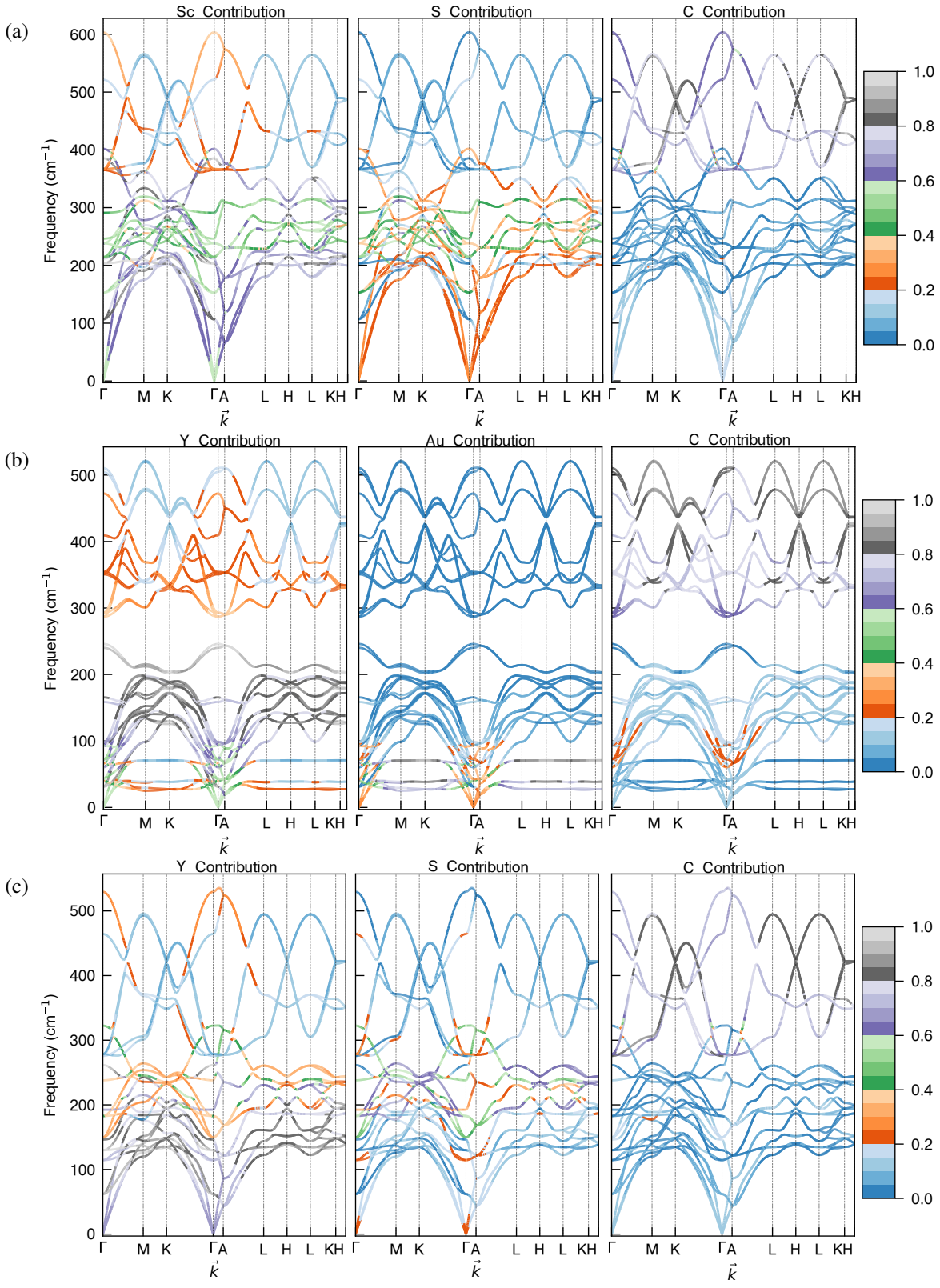
(a)
Sc Contribution
S Contribution
C Contribution
Frequency (cm$^{-1}$)
0
100
200
300
400
500
600
Γ M K Γ A L H L KH
$\vec{k}$
1.0
0.8
0.6
0.4
0.2
0.0
(b)
Y Contribution
Au Contribution
C Contribution
(c)
Y Contribution
S Contribution
C Contribution

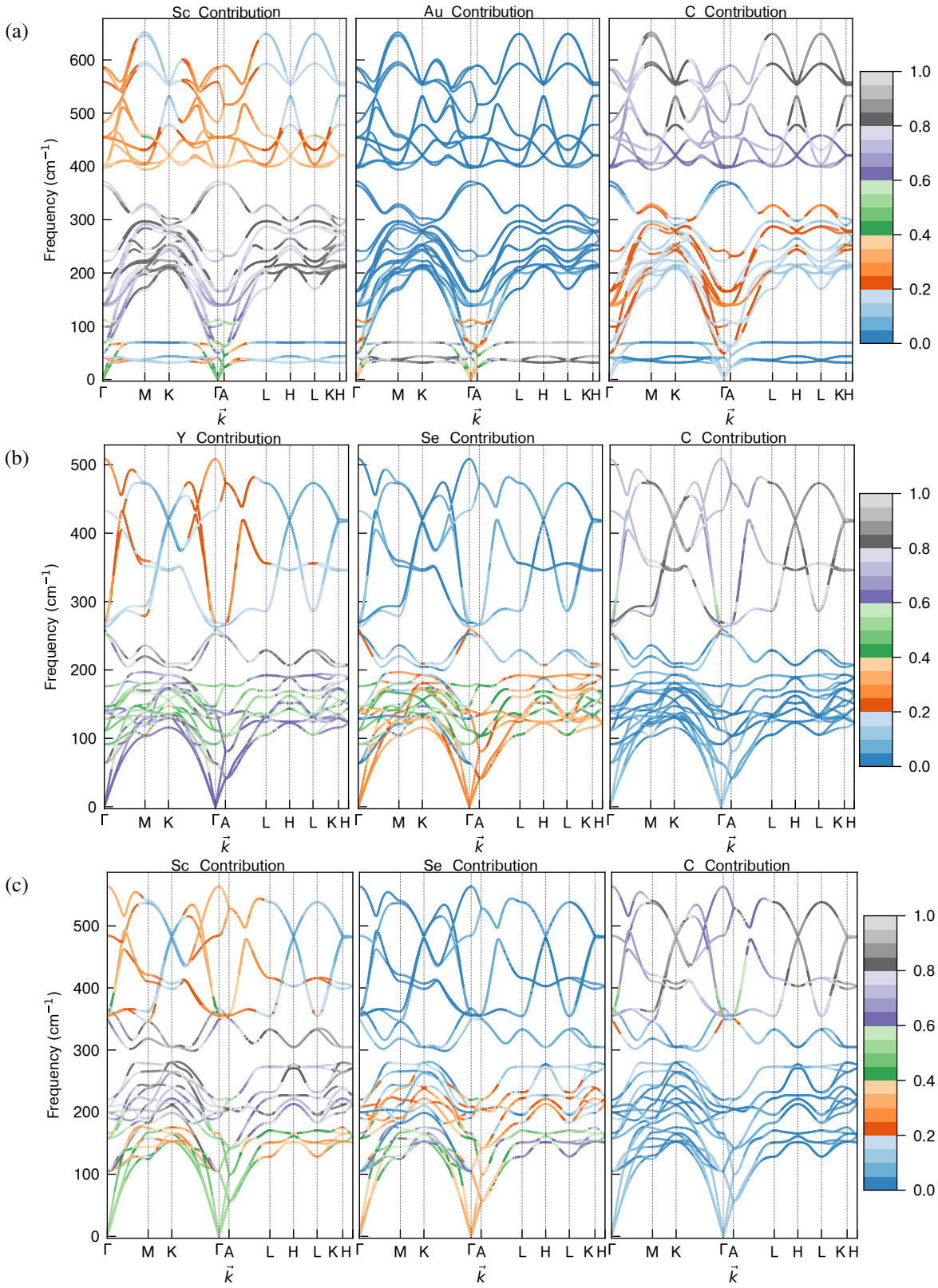


FIG. S3: The projected phonon dispersion curve.

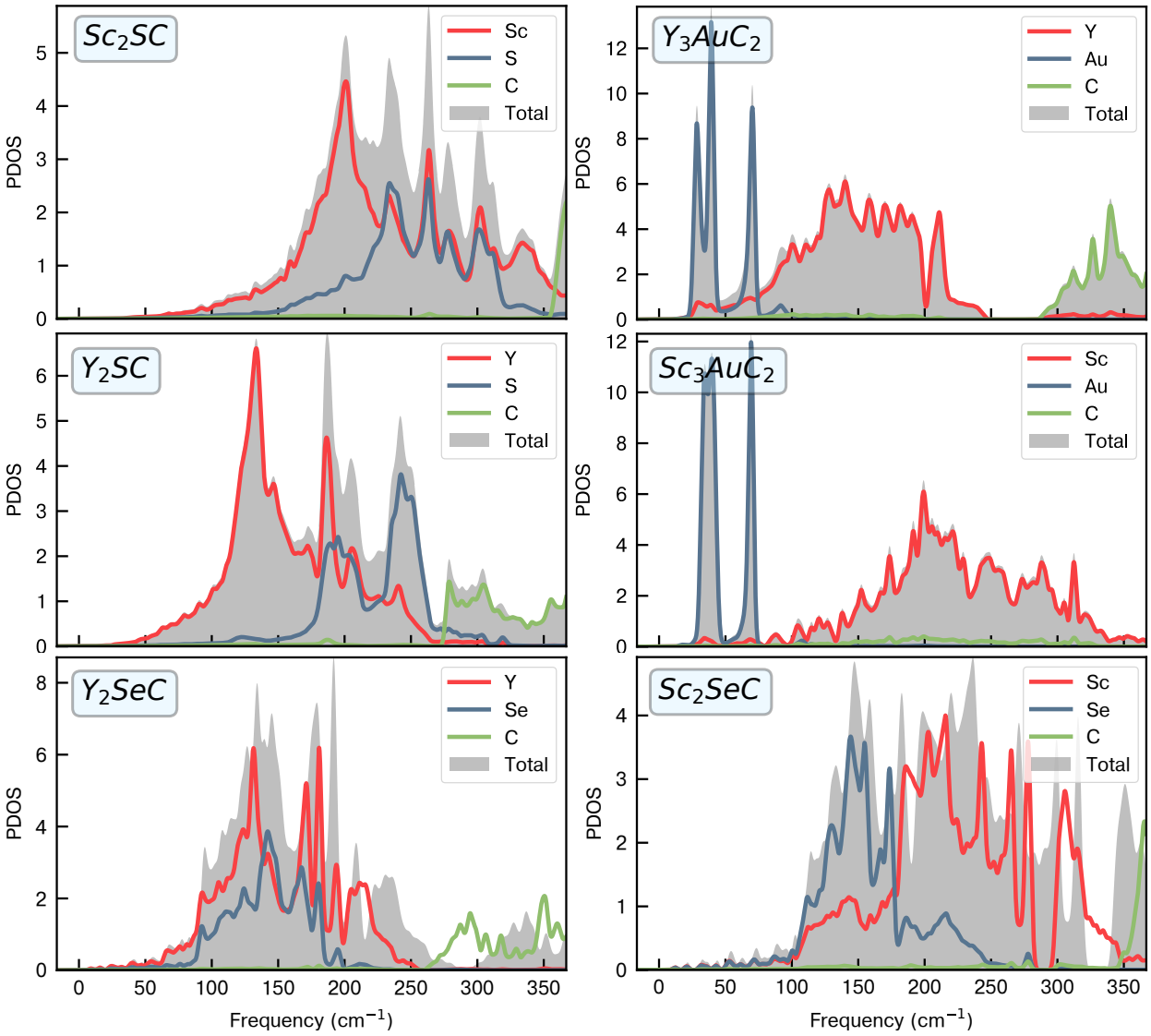


FIG. S4: The phonon projected density of states for all structures.

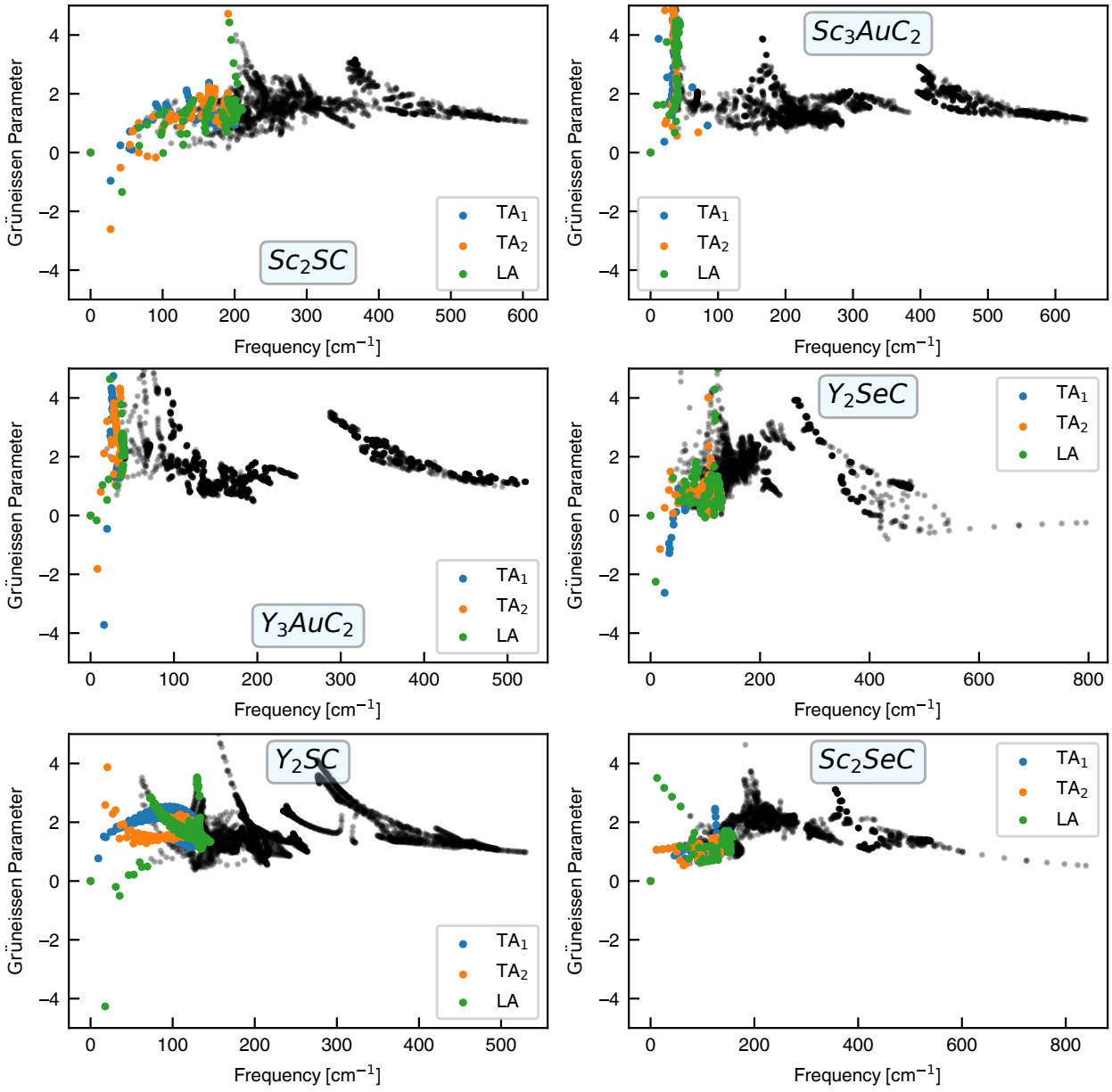


FIG. S5: The Grünisen parameter of all structures.

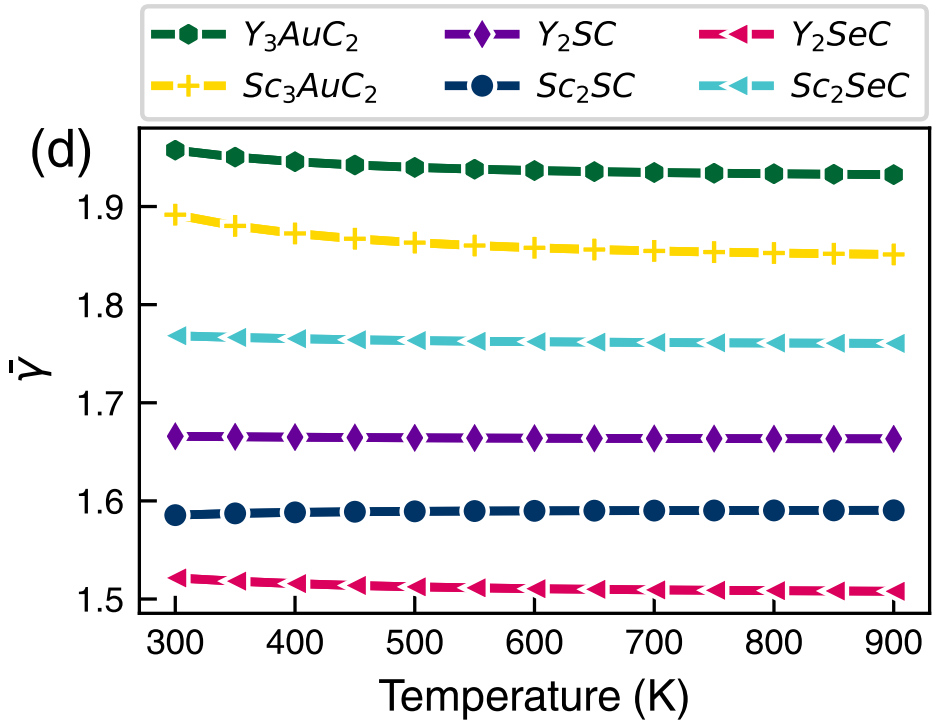


FIG. S6: The average Grünisen parameter of all structures.

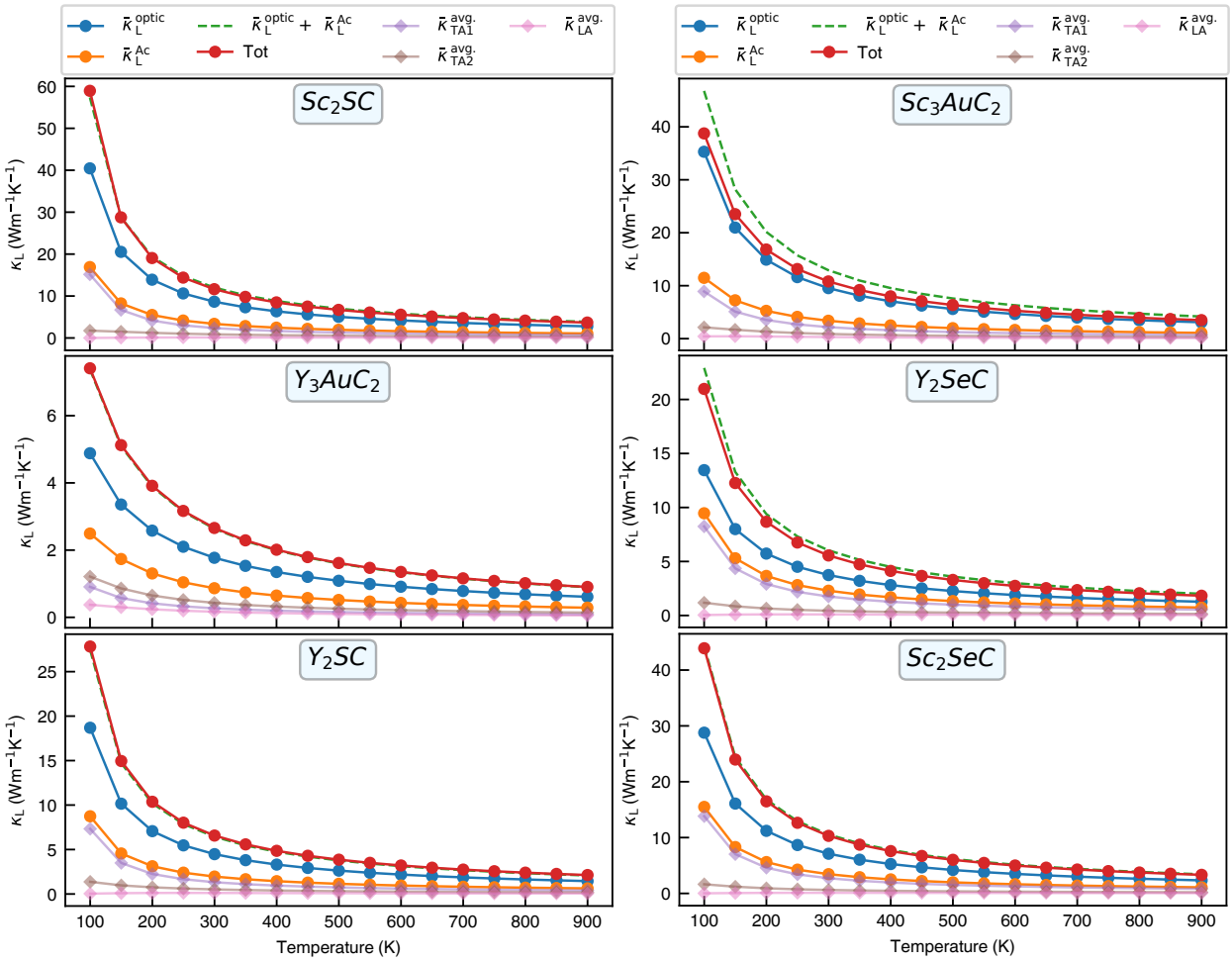


FIG. S7: Lattice thermal conductivity decomposed on various components.

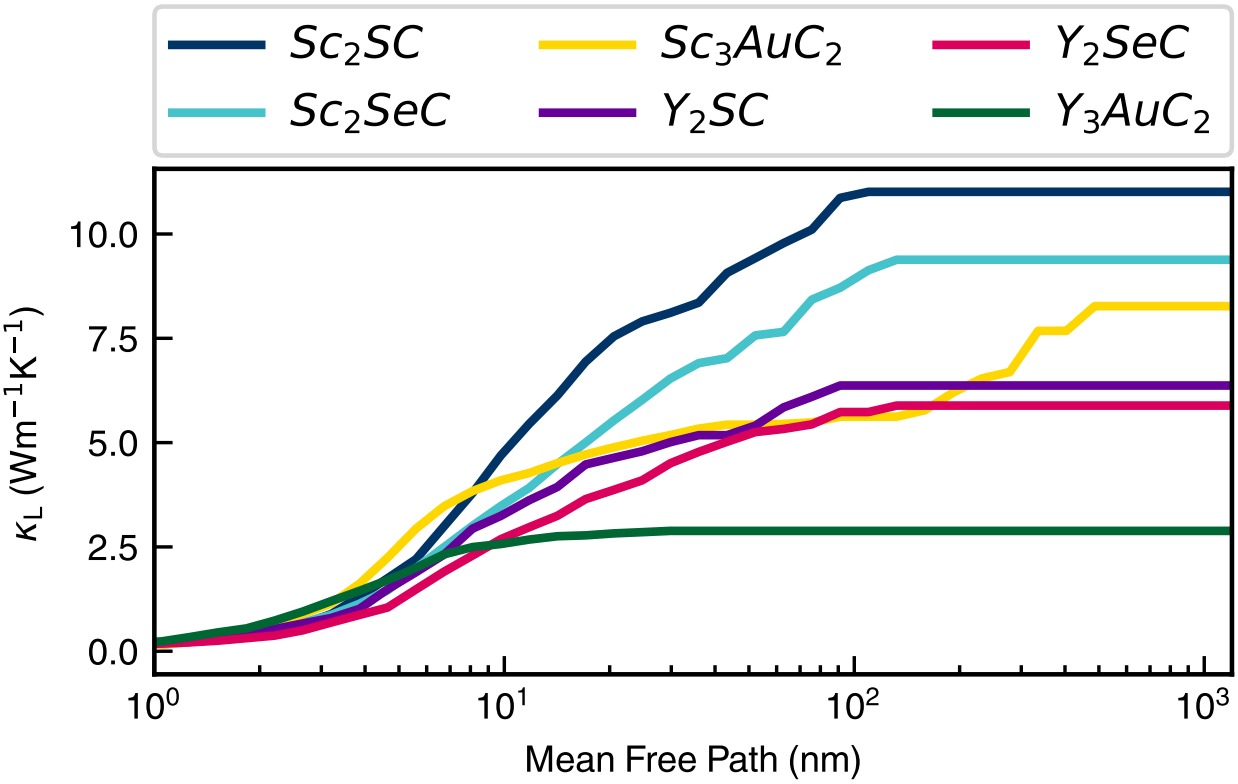


FIG. S8: The accumulative kappa Vs mean free path for all structures.

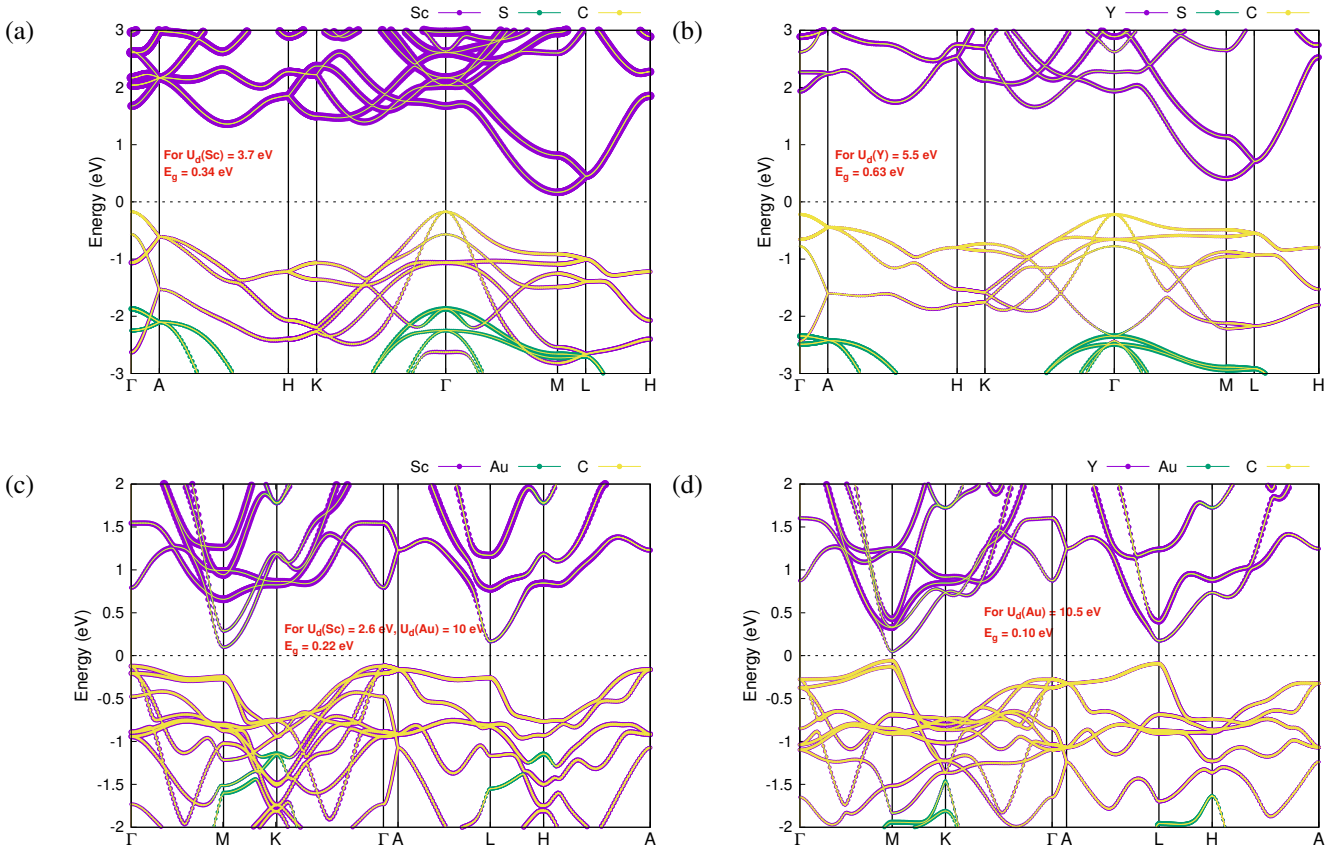


FIG. S9: The band structure of (a) $Sc_2SC$, (b) $Y_2SC$, (c) $Sc_3AuC_2$, and (d) $Y_3AuC_2$ using appropriate U values.

The band structure of four MAX phases obtained using GGA+U method [4] is given in Figure S9. As a representation, the ab-initio parameters of $Sc_2SC$ and $Y_2SC$ used in the transport code, AMMCR [3, 5, 6] are given in Table S1.

TABLE S1: Material parameters used for $Sc_2SC$ and $Y_2SC$

| Parameters | $Sc_2SC$ | $Y_2SC$ |
|---|---|---|
| Acoustic deformation potentials, $D_A(eV)$ : | | |
| $D_{A,LA}$ | 7.90 | 5.74 |
| $D_{A,TA}$ | 7.90 | 5.74 |
| $D_{A,ZA}$ | 6.80 | 4.36 |
| Elastic modulus, $C_A(dynes/cm^2)$ | | |
| $C_{A,LA}$ | 2.76 x $10^{12}$ | 2.20 x $10^{12}$ |
| $C_{A,TA}$ | 2.76 x $10^{12}$ | 2.20 x $10^{12}$ |
| $C_{A,ZA}$ | 2.68 x $10^{12}$ | 2.17 x $10^{12}$ |
| Polar optical phonon frequency $\omega_{pop}(THz)$ | | |
| $\omega_{pop,LO}$ | 6.87 | 5.67 |
| $\omega_{pop,TO}$ | 6.87 | 5.67 |
| $\omega_{pop,ZO}$ | 8.76 | 7.45 |
| High frequency dielectric constant, $\epsilon_\infty$ | 11.49 | 9.62 |
| Low frequency dielectric constant, $\epsilon_0$ | 26.34 | 23.50 |

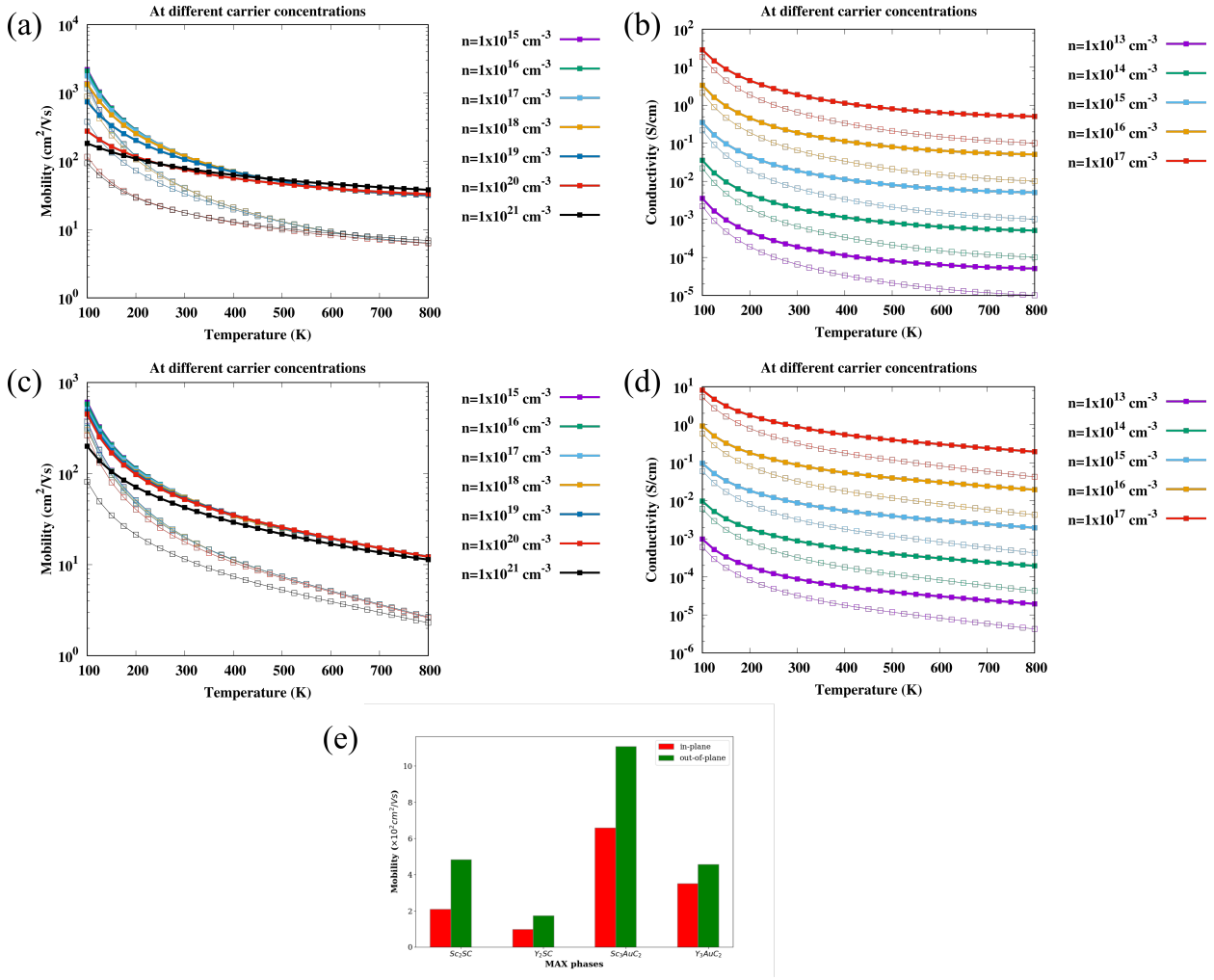


FIG. S10: Electron mobility and conductivity of (a,b) $Sc_2SC$ (first row) and (c,d) $Y_2SC$ (second row) MAX phases. The filled and empty squares represent the property calculated using Rode's method and RTA respectively. (e) The bar plot representing in-plane and out-of-plane mobility of $Sc_2SC$, $Y_2SC$, $Sc_3AuC_2$ and $Y_3AuC_2$ at 300 K and an electron concentration of $5\times10^{15}$ $cm^{-3}$.

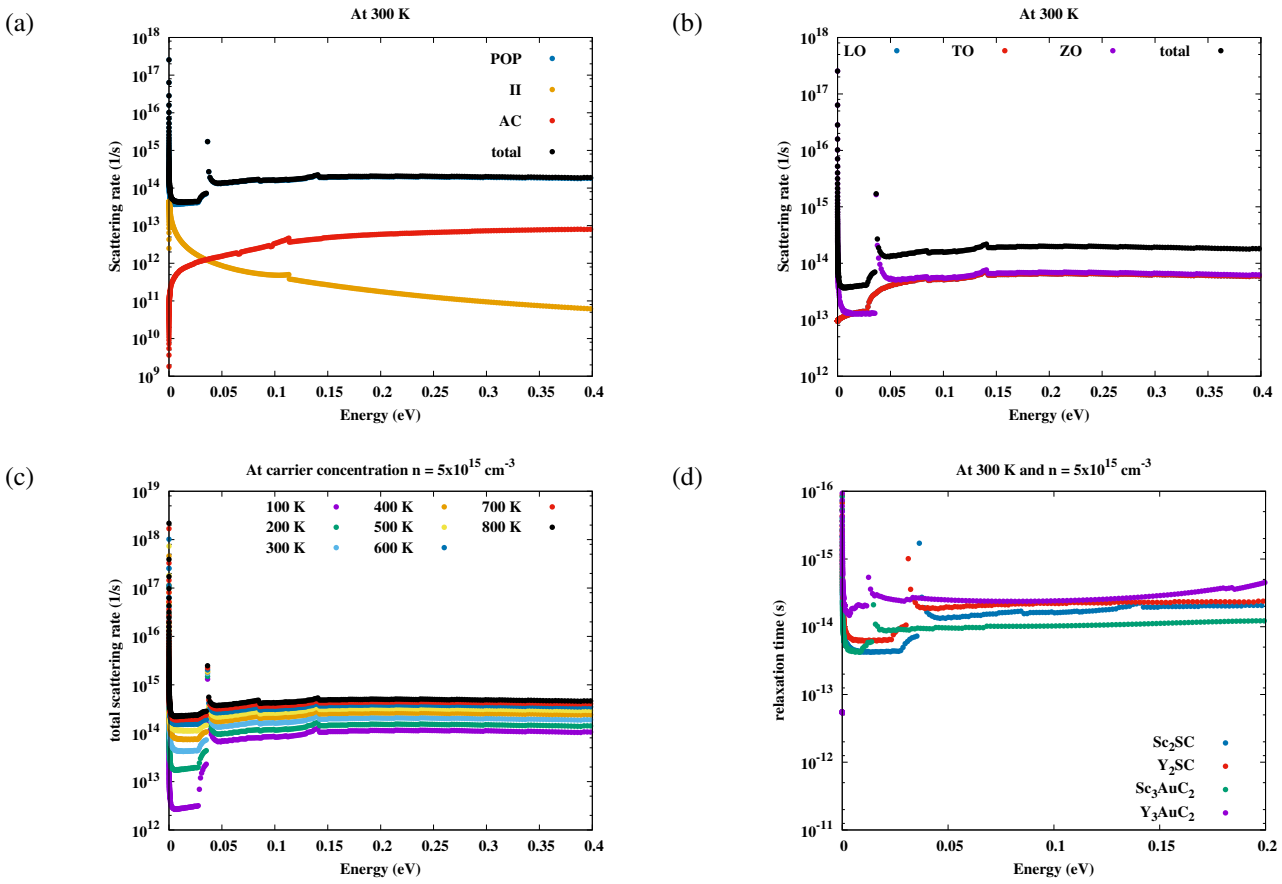


FIG. S11: (a) Total scattering rate and (b) contribution of LO, TO and ZO modes to the scattering rate of $Sc_2SC$ at 300 K for an electron concentration of $5 \times 10^{15}$ cm$^{-3}$. (c) Total scattering rate of $Sc_2SC$ as a function of temperature. (d) Average relaxation time of $Sc_2SC$, $Y_2SC$, $Sc_3AuC_2$ and $Y_3AuC_2$.

In Figure S11, the scattering rate of $Sc_2SC$ for an electron concentration of $5 \times 10^{15}$ cm$^{-3}$ is provided. Also, the average relaxation time for all the four MAX phases are shown.

The electron mobility and conductivity of four semiconducting MAX phases are calculated using AMMCR code, which employs Rode's iterative method. These values are compared with those obtained using relaxation time approximation (RTA). For $Sc_2SC$ and $Y_2SC$, the corresponding plots are given in Figure S10.

TABLE S2: Calculated S($\mu VK^{-1}$ ), PF = $S^2\sigma/\tau$ ($10^{14}mW/mK^2s$ ), $\kappa_l$($\mathrm{Wm^{-1}K^{-1}}$) and zT for all structures along z-axis at the different tempretures.

| | **T = 300K** | | | | **T = 500K** | | | |
|---|---|---|---|---|---|---|---|---|
| | $S$ | $S^2\sigma/\tau$ | $\kappa_l$ | $zT$ | $S$ | $S^2\sigma/\tau$ | $\kappa_l$ | $zT$ |
| ***$Sc_2SC$*** | | | | | | | | |
| $p-type$ | 584.97 | 0.46 | 12.89 | 0.006 | 376.10 | 0.96 | 7.49 | 0.037 |
| $n-type$ | -583.72 | 0.44 | 12.89 | 0.006 | -377.27 | 1.2 | 7.49 | 0.041 |
| ***$Y_2SC$*** | | | | | | | | |
| $p-type$ | 1300.27 | 1.05 | 7.69 | 0.02 | 795.10 | 2.10 | 4.53 | 0.085 |
| $n-type$ | -1279.11 | 0.53 | 7.69 | 0.01 | -762.79 | 1.17 | 4.53 | 0.05 |
| ***$Sc_2SeC$*** | | | | | | | | |
| $p-type$ | 235.22 | 0.35 | 12.16 | 0.009 | 176.26 | 0.65 | 7.08 | 0.043 |
| $n-type$ | -241.04 | 0.48 | 12.16 | 0.011 | -195.30 | 3.95 | 7.08 | 0.063 |
| ***$Y_2SeC$*** | | | | | | | | |
| $p-type$ | 592.20 | 0.49 | 4.89 | 0.023 | 378.71 | 1.00 | 2.94 | 0.15 |
| $n-type$ | -566.37 | 0.50 | 4.89 | 0.02 | -367.70 | 1.04 | 2.94 | 0.14 |
| ***$Sc_3AuC_2$*** | | | | | | | | |
| $p-type$ | 694.50 | 2.96 | 28.45 | 0.02 | 406.50 | 4.01 | 16.73 | 0.073 |
| $n-type$ | -580 | 1.63 | 28.45 | 0.01 | -351.20 | 2.84 | 16.73 | 0.047 |
| ***$Y_3AuC_2$*** | | | | | | | | |
| $p-type$ | 556.73 | 0.4 | 2.21 | 0.07 | 319.15 | 0.55 | 1.3 | 0.27 |
| $n-type$ | -604.07 | 0.78 | 2.21 | 0.14 | -375.30 | 1.09 | 1.3 | 0.50 |

TABLE S3: Calculated S($\mu VK^{-1}$ ), PF = $S^2\sigma/\tau$ ($10^{14}mW/mK^2s$ ), $\kappa_l$($\mathrm{Wm^{-1}K^{-1}}$) and zT for all structures along ab-lattice at the different tempretures.

| | **T = 300K** | | | | **T = 500K** | | | |
|---|---|---|---|---|---|---|---|---|
| | $S$ | $S^2\sigma/\tau$ | $\kappa_l$ | $zT$ | $S$ | $S^2\sigma/\tau$ | $\kappa_l$ | $zT$ |
| ***$Sc_2SC$*** | | | | | | | | |
| $p-type$ | 522.45 | 0.45 | 11.01 | 0.01 | 315.90 | 0.93 | 6.31 | 0.042 |
| $n-type$ | -639.30 | 1.69 | 11.01 | 0.026 | -424.50 | 3.23 | 6.31 | 0.14 |
| ***$Y_2SC$*** | | | | | | | | |
| $p-type$ | 1257.20 | 2.47 | 6.36 | 0.045 | 735.17 | 4.84 | 3.72 | 0.19 |
| $n-type$ | -1313.17 | 1.42 | 6.36 | 0.032 | -811.53 | 2.74 | 3.72 | 0.16 |
| ***$Sc_2SeC$*** | | | | | | | | |
| $p-type$ | 180.13 | 0.40 | 9.38 | 0.013 | 135.41 | 0.83 | 5.48 | 0.065 |
| $n-type$ | -296.34 | 1.85 | 9.38 | 0.055 | -234.05 | 3.42 | 5.48 | 0.25 |
| ***$Y_2SeC$*** | | | | | | | | |
| $p-type$ | 522.80 | 1.78 | 5.88 | 0.023 | 318.77 | 3.28 | 3.46 | 0.13 |
| $n-type$ | -632.18 | 1.55 | 5.88 | 0.072 | -415.65 | 2.91 | 3.46 | 0.33 |
| ***$Sc_3AuC_2$*** | | | | | | | | |
| $p-type$ | 758.25 | 8.48 | 8.27 | 0.17 | 495.75 | 12.22 | 4.92 | 0.66 |
| $n-type$ | -632.83 | 1.74 | 8.27 | 0.042 | -379.92 | 3.77 | 4.92 | 0.22 |
| ***$Y_3AuC_2$*** | | | | | | | | |
| $p-type$ | 635.90 | 5.28 | 2.88 | 0.57 | 408.07 | 8.45 | 1.77 | 1.73 |
| $n-type$ | -556.28 | 1.98 | 2.88 | 0.25 | -331.85 | 3.56 | 1.77 | 0.88 |

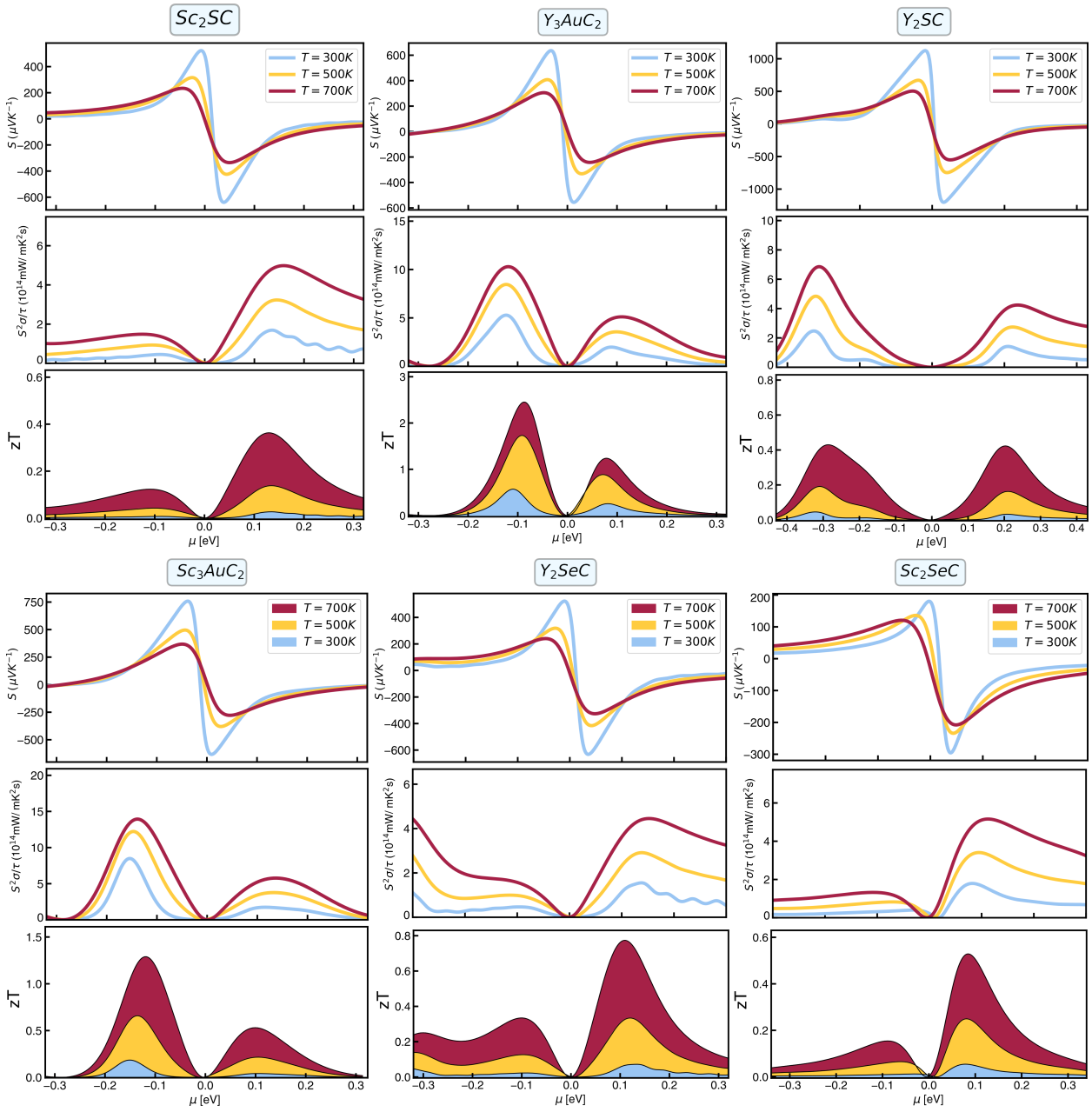


FIG. S12: Seebeck and power factor and $zT$ parameter for all structures.

# Coordinates of $Sc_2SC$

POSCAR of Sc2SC

1.0

3.4391777515 0.0000000000 0.0000000000

-1.7195888758 2.9784153010 0.0000000000

0.0000000000 0.0000000000 11.9092426300

Sc S C

4 2 2

Direct

0.666666985 0.333332986 0.602460027

0.666666985 0.333332986 0.897539973

0.333332986 0.666666985 0.102459997

0.333332986 0.666666985 0.397540003

0.333332986 0.666666985 0.750000000

0.666666985 0.333332986 0.250000000

0.000000000 0.000000000 0.500000000

0.000000000 0.000000000 0.000000000

# Coordinates of $Y_2SC$

POSCAR of Y2SC

1.0

3.7083451748 0.0000000000 0.0000000000

-1.8541725874 3.2115211274 0.0000000000

0.0000000000 0.0000000000 12.8999385834

Y S C

4 2 2

Direct

0.666666985 0.333332986 0.604048014

0.666666985 0.333332986 0.895951986

0.333332986 0.666666985 0.104047999

0.333332986 0.666666985 0.395951986

0.333332986 0.666666985 0.750000000

0.666666985 0.333332986 0.250000000

0.000000000 0.000000000 0.500000000

0.000000000 0.000000000 0.000000000

# Coordinates of $Sc_2SeC$

POSCAR of Sc2SeC

1.0

3.4966380596 0.0000000000 0.0000000000

-1.7483190298 3.0281773875 0.0000000000

0.0000000000 0.0000000000 12.3083686829

Sc Se C

4 2 2

Direct

0.666666985 0.333332986 0.597823977

0.666666985 0.333332986 0.902176023

0.333332986 0.666666985 0.097824000

0.333332986 0.666666985 0.402175993

0.333332986 0.666666985 0.750000000

0.666666985 0.333332986 0.250000000

0.000000000 0.000000000 0.500000000

0.000000000 0.000000000 0.000000000

# Coordinates of $Y_2SeC$

POSCAR of Y2SeC

1.0

3.7715880871 0.0000000000 0.0000000000

-1.8857940435 3.2662910960 0.0000000000

0.0000000000 0.0000000000 13.3069391251

Y Se C

4 2 2

Direct

0.666666985 0.333332986 0.600241005

0.666666985 0.333332986 0.899758995

0.333332986 0.666666985 0.100240998

0.333332986 0.666666985 0.399758995

0.333332986 0.666666985 0.750000000

0.666666985 0.333332986 0.250000000

0.000000000 0.000000000 0.500000000

0.000000000 0.000000000 0.000000000

# Coordinates of $Sc_3AuC_2$

POSCAR of Sc3AuC2

1.0

3.3747251034 0.0000000000 0.0000000000

-1.6873625517 2.9225976703 0.0000000000

0.0000000000 0.0000000000 19.1152229309

Sc Au C

6 2 4

Direct

0.000000000 0.000000000 0.000000000

0.000000000 0.000000000 0.500000000

0.333332986 0.666666985 0.130154997

0.666666985 0.333332986 0.630155027

0.666666985 0.333332986 0.869844973

0.333332986 0.666666985 0.369845003

0.000000000 0.000000000 0.250000000

0.000000000 0.000000000 0.750000000

0.333332986 0.666666985 0.925032973

0.666666985 0.333332986 0.425033003

0.666666985 0.333332986 0.074966997

0.333332986 0.666666985 0.574967027

# Coordinates of $Y_3AuC_2$

POSCAR of Y3AuC2

1.0

3.6488833427 0.0000000000 0.0000000000

-1.8244416714 3.1600256703 0.0000000000

0.0000000000 0.0000000000 20.2883396149

Y Au C

6 2 4

Direct

0.000000000 0.000000000 0.000000000

0.000000000 0.000000000 0.500000000

0.333332986 0.666666985 0.135432005

0.666666985 0.333332986 0.635432005

0.666666985 0.333332986 0.864567995

0.333332986 0.666666985 0.364567995

0.000000000 0.000000000 0.250000000

0.000000000 0.000000000 0.750000000

0.333332986 0.666666985 0.922215998

0.666666985 0.333332986 0.422215998

0.666666985 0.333332986 0.077784002

0.333332986 0.666666985 0.577784002

[1] D. L. Rode, *Semiconductors and Semimetals* (Academic Press, New York, **1975**), Chapter 1.

[2] A. Faghaninia, J. W. Ager III, C. S. Lo, Phys. Rev. B **2015**, 91, 235123.

[3] A. K. Mandia, B. Muralidharan, J. -H. Choi, S. -C. Lee, S. Bhattacharjee, Comput. Phys. Commun. **2021**, 259, 107697.

[4] S. L. Dudarev, G. A. Botton, S. Y. Savrasov, C. J. Humphreys, A. P. Sutton, Phys. Rev. B **1998**, 57, 1505.

[5] A. K. Mandia, R. Patnaik, B. Muralidharan, S. -C. Lee, S. Bhattacharjee, J. Phys.: Condens. Matter **2019**, 31, 345901.

[6] S. Chakrabarty, A. K. Mandia, B. Muralidharan, S. -C. Lee, S. Bhattacharjee, J. Phys.: Condens. Matter **2019**, 32, 135704.

**Some additional discussion regarding relaxation time:**

Though there is currently no experimental data available on semiconducting MAX phases as they have not been synthesized. Nevertheless, we have a reliable estimation of the relaxation time in metallic MAX phases based on our previous estimation using experimental results for electrical conductivity, which can be found in the supporting information file of Physical Chemistry Chemical Physics 16, 7841(2014). Below, we have summarized the results.

**References for the experimental results in the follwoing table:**


[1] M. W. Barsoum, M. Ali, T. El-Raghy, *Met. Mater. Trans. A* 2000, **31**, 1857.
[2] W. B. Tian, P. L. Wang, G. J. Zhang, Y. M. Kan, Y. X. Li, D. S. Yan, *Scr. Mater.* 2006, **54**, 841.
[3] M. W. Barsoum, D. Brodkin, T. ElRaghy, *Scr. Mater.* 1997, **36**, 535.
[4] M. W. Barsoum, *Prog. Solid State Chem.* 2000, **28**, 201.
[5] T. H. Scabarozi, S. Amini, P. Finkel, O. D. Leaffer, J. E. Spanier, M. W. Barsoum, M. Drulis, H. Drulis, W. M. Tambussi, J. D. Hettinger, S. E. Lofland, *J. Appl. Phys.* 2008, **104**, 033502.
[6] M. W. Barsoum, J. Golczewski, H. J. Seifert, F. Aldinger, *J. Alloys Compd.* 2002, **340**, 173.
[7] T. El-Raghy, S. Chakraborty, M. W. Barsoum, *J. Eur. Ceram. Soc.* 2000, **20**, 2619.
[8] J. D. Hettinger, S. E. Lofland, P. Finkel, T. Meehan, J. Palma, K. Harrell, S. Gupta, A. Ganguly, T. El-Raghy, M. W. Barsoum, *Phys. Rev. B* 2005, **72**, 115120.
[9] M. W. Barsoum, G. Yaroschuk, S. Tyagi, *Scr. Mater.* 1977, **37**, 1583.
[10] M. W. Barsoum, I. Salama, T. El-Raghy, J. Golczewski, W. D. Porter, H. Wang, H. J. Seifert, F. Aldinger, *Met. Mater. Trans. A* 2002, **33**, 2775.
[11] Z. J. Lin, M. J. Zhuo, Y. C. Zhou, M. S. Li, J. Y. Wang, *J. Am. Ceram. Soc.* 2006, **89**, 3765.
[12] C. F. Hu, L. F. He, J. Zhang, Y. W. Bao, J. Y. Wang, M. S. Li, Y. C. Zhou, *J. Eur. Ceram. Soc.* 2008, **28**, 1679.


| $M_2AX$ Phase | a (Å) | c (Å) | Experimental σ (1/μΩ.m) | Calculated σ/ τ (1/Ω.m.s) | Estimated τ (s) |
|---|---|---|---|---|---|
| $Ti_2AlC$ | 3.069, 3.051[1] | 13.737, 13.637[1] | 2.7[1,2], 2.8[1] | $2.797\times10^{20}$ | $1.036\times10^{-14}$, $0.999\times10^{-14}$ |
| $Ti_2AlN$ | 2.997, 2.989[1] | 13.644, 13.614[1] | 3.2[3], 4.00[1] | $2.700\times10^{20}$ | $0.844\times10^{-14}$, $0.675\times10^{-14}$ |
| $Ti_2SC$ | 3.205, 3.216[4] | 11.257, 11.22[4] | 1.923[5] | $1.450\times10^{20}$ | $0.754\times10^{-14}$ |
| $Ti_2GeC$ | 3.094, 3.07[4] | 12.991, 12.93[4] | 4.4[3] | $3.995\times10^{20}$ | $0.908\times10^{-14}$ |
| $Ti_2InC$ | 3.148, 3.134[4] | 14.208, 14.077[4] | 5.000[6] | $2.367\times10^{20}$ | $0.473\times10^{-14}$ |
| $Ti_2SnC$ | 3.178, 3.163[4] | 13.777, 13.679[4] | 4.545[7] | $3.944\times10^{20}$ | $0.868\times10^{-14}$ |
| $V_2AlC$ | 2.906, 3.1[4] | 13.104, 13.83[4] | 4.000[8] | $3.095\times10^{20}$ | $0.774\times10^{-14}$ |
| $Cr_2AlC$ | 2.847, 2.863[2] | 12.671, 12.814[2] | 1.389[8], 1.4[2] | $2.998\times10^{20}$ | $2.129\times10^{-14}$, $2.158\times10^{-14}$ |
| $Zr_2SnC$ | 3.390, 3.358[4] | 14.684, 14.57[4] | 3.571[7], 7.00[9] | $4.475\times10^{20}$ | $1.253\times10^{-14}$, $0.639\times10^{-14}$ |
| $Zr_2PbC$ | 3.418, 3.38[4] | 14.926, 14.66[4] | 2.778[7] | $4.455\times10^{20}$ | $1.604\times10^{-14}$ |
| $Nb_2AlC$ | 3.116, 3.1[4] | 13.932, 13.8[4] | 3.448[10] | $4.174\times10^{20}$ | $1.210\times10^{-14}$ |
| $Nb_2SnC$ | 3.268, 3.214[4] | 13.888, 13.802[4] | 2.222[7], 4.00[9] | $6.070\times10^{20}$ | $2.732\times10^{-14}$, $1.517\times10^{-14}$ |
| $Hf_2InC$ | 3.324, 3.309 | 14.890, 14.723 | 5.263[6] | $3.270\times10^{20}$ | $0.621\times10^{-14}$ |
| $Hf_2SnC$ | 3.345, 3.320[4] | 14.449, 14.388[4] | 2.222[7], 2.4[9] | $5.379\times10^{20}$ | $2.421\times10^{-14}$, $2.241\times10^{-14}$ |
| $Hf_2PbC$ | 3.379, 3.55[7] | 14.680, 14.46[7] | 13.333[7] | $5.391\times10^{20}$ | $0.404\times10^{-14}$ |
| $Ta_2AlC$ | 3.093, 3.079[11] | 13.957 13.860[11] | 3.91[12] | $4.803\times10^{20}$ | $1.228\times10^{-14}$ |

As seen in the above Table, we conducted an extensive search in the literature and gathered data on the electrical conductivity (σ) for 16 different M2AX systems, as listed in the table below. Using Boltzmann theory and first-principles calculations, we determined the σ/τ for these $M_2AX$ systems and estimated the relaxation time (τ) by fitting the experimental data of σ. The estimated relaxation time ranges from $0.4\times10^{-14}$s to $2.7\times10^{-14}$s, as shown in the table. Despite limitations in the number of conductivity measurements and the scattered nature of the data for different $M_2AX$ systems, which involve various transition metals (M), interlayer elements (A), and X atoms (carbon or nitrogen), we can conclude that the average relaxation time of approximately $1.251\times10^{-14}$s can be considered a reliable value for the relaxation time in all the considered $M_2AX$ systems with similar hexagonal structures. This value is comparable to the relaxation time obtained for semiconducting MAX phases through scattering theory.

Moreover, we have tested the Rode's method of estimating mobility on other known bulk semiconductors like CdS and ZnSe. The results are in good agreement with available/existing experimental data and are published [Computer Physics Communications 2559, 107697 (2021) and J. Phys.: Condens. Matter 31, 345901 (2019)]. These mobilities are obtained from the determination of scattering rate for each scattering mechanism that is significant to the material. The average relaxation time is calculated from these scattering rates. If the mobilities match well with experimental data, we expect the relaxation time to be correct.

The mobility of CdS as a function of temperature for a carrier concentration of 6.9 x $10^{15}$ $cm^{-3}$ [Computer Physics Communications 2559, 107697 (2021)] is given in the following figure. The figure shows good qualitative and quantitative agreement between experimental and calculated curves. The contribution of each scattering mechanism towards mobility is also provided. In Figure 1(b), the red curve corresponds to experimental data and the black line represents the total mobility due to acoustic deformation potential, piezoelectric, polar optical phonon and ionized impurity scattering.

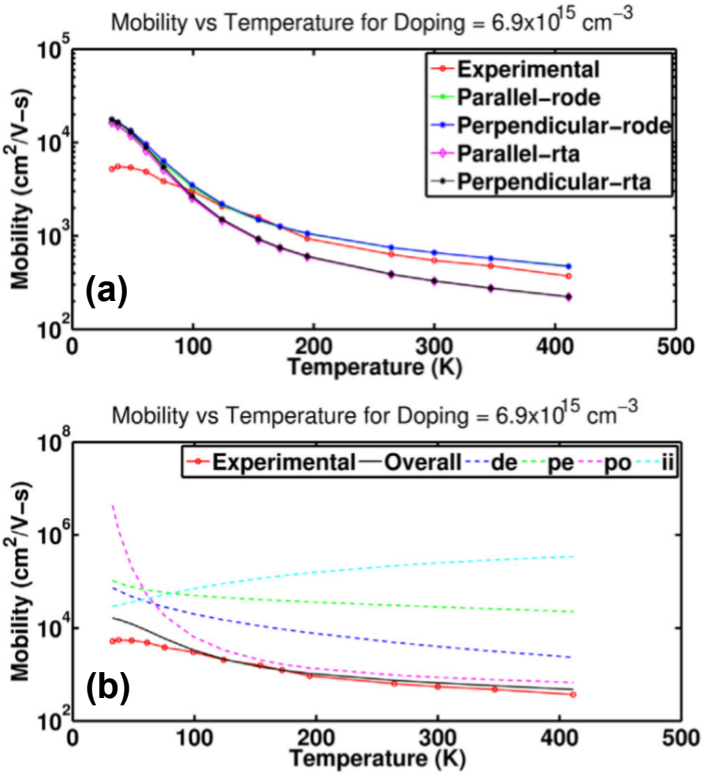


**Figure 1: (a) Calculated and experimental measured mobility of CdS as a function of temperature for a specific carrier concentration. (b) The contribution of different scattering mechanisms towards mobility for the same [Computer Physics Communications 2559, 107697 (2021), Phys. Rev. 169, 577 (1968)].**

For ZnSe, the electron mobility is calculated for three different samples with different carrier concentrations over a wide temperature range. The donor and acceptor concentrations of the samples are taken as shown in Table 1. As can be seen in the mobility versus temperature plots, the Rode's method gives mobility which are in better agreement with experimental values compared to those obtained using relaxation time approximation.

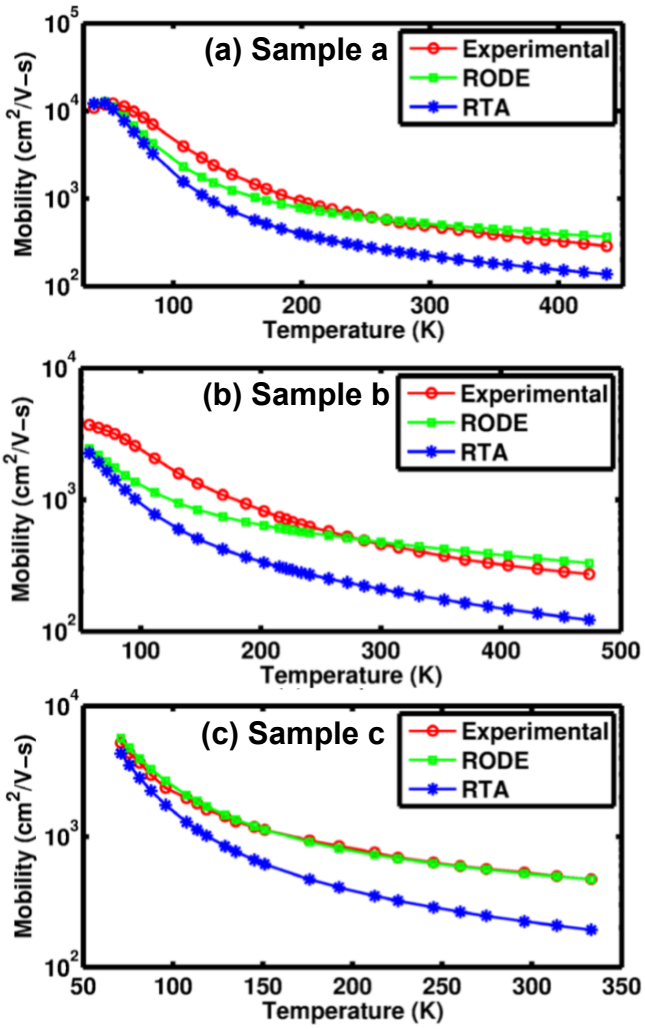


**Figure 2: Calculated and experimentally measured mobility of ZnSe with temperature variation at different carrier concentrations [J. Phys.: Condens. Matter 31, 345901 (2019)]. The details about donor and acceptor concentrations are given in Table 1.**

**Table 1: Carrier of different experimentally fabricated n-ZnSe samples.**

| Sample | $N_D$ - $N_A$ ($cm^{-3}$) | Donor $N_D$ ($cm^{-3}$) | Acceptor $N_A$ ($cm^{-3}$) |
|---|---|---|---|
| a [#] | $1 \times 10^{15}$ | $2.9 \times 10^{15}$ | $1.9 \times 10^{15}$ |
| b [$] | $1.1 \times 10^{16}$ | $6 \times 10^{16}$ | $4.9 \times 10^{16}$ |
| c [*] | $6.3 \times 10^{15}$ | $7.5 \times 10^{15}$ | $1.2 \times 10^{15}$ |

[#J. Appl. Phys. 42, 1204 (1971), $J. Phys.: Condens. Matter 18, 8113 (2006), *Phys. Status Solidi b 238, 45 (2003)]

Finally, the acoustic deformation potential is calculated using standard procedure followed in other theoretical works based on Bardeen and Shockley proposition (Phys. Rev. 80, 72 (1950)). $E_D$ is the deformation potential constant. It represents the shift of the conduction band edge (i.e. conduction band minima for electrons) induced by the strains and is defined

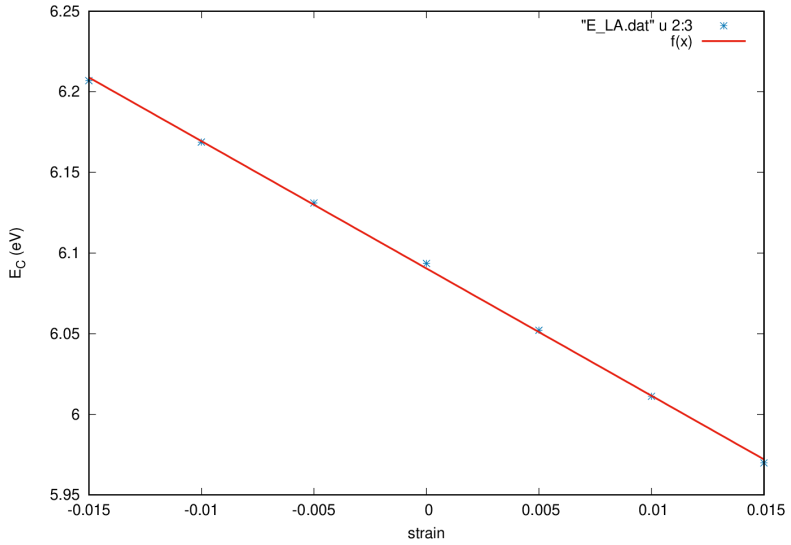


**Figure 3: Linear fit of conduction band edge of $Sc_2SC$ MAX phase compound as a function of small strain.**

as $E_D = \partial E_{CBM}/\partial\varepsilon$. The strain ε is given by $(l-l_0)/l_0$, where l and $l_0$ are the strained and equilibrium lattice parameters respectively. For $Sc_2SC$ MAX phase, the shift of conduction band edge as a function of strain (for the strain in the x-direction) is given above.

function used for fitting: $f(x) = E(\varepsilon) = a\varepsilon+b$

| Final set of parameters | | Asymptotic Standard Error | |
|---|---|---|---|
| a | = -7.89714 | +/- 0.07763 | (0.983%) |
| b | = 6.09046 | +/- 0.0007763 | (0.01275%) |

$E_{1x} = \partial E/\partial\varepsilon = -7.897$

Please note that it is the polar optical phonon (POP) scattering rate which is most dominant in the MAX phases considered. The Rode's method of estimating mobility is found to be good for polar

semiconductors as explained in Refs. [Computer Physics Communications 2559, 107697 (2021) and J. Phys.: Condens. Matter 31 345901 (2019)].

**To verify the absence of imaginary modes, the inset shows a zoomed-in view of the phonon frequencies at the Gamma point region. It clearly demonstrates that there are no imaginary phonon modes in these structures.**

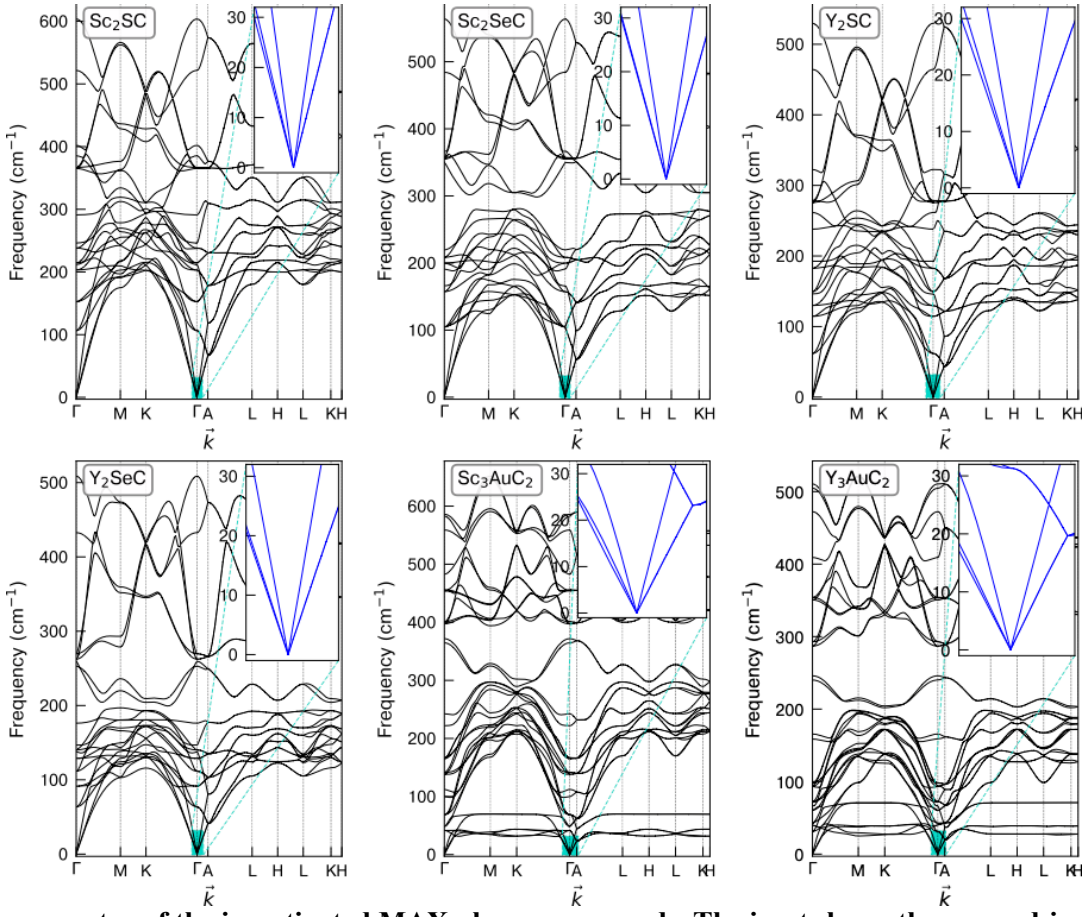


**Phonon spectra of the investigated MAX phase compounds. The inset shows the zoomed-in view at the zone centers.**